
Morphological evidence for a past minor merger in the Seyfert galaxy NGC 1068*

Ichi TANAKA¹, Masafumi YAGI,² and Yoshiaki TANIGUCHI³

¹Subaru Telescope, National Astronomical Observatory of Japan, 650 North A'ohoku Place, Hilo, Hawaii, 96720, U.S.A.

²National Astronomical Observatory of Japan, 2-21-1, Osawa, Mitaka, Tokyo, 181-8588, Japan

³The Open University of Japan, 2-11 Wakaba, Mihama-ku, Chiba 261-8586, Japan

*E-mail: ichi@naoj.org, YAGI.Masafumi@nao.ac.jp, yoshiaki-taniguchi@ouj.ac.jp

Received 2017 July 13; Accepted 2017 August 21

Abstract

Deep optical imaging with both Hyper Suprime-Cam and Suprime-Cam on the 8.2 m Subaru Telescope reveals a number of outer faint structures around the archetypical Seyfert galaxy NGC 1068 (M 77). We find three ultra diffuse objects (UDOs) around NGC 1068. Since these UDOs are located within the projected distance of 45 kpc from the center of NGC 1068, they appear to be associated with NGC 1068. Hereafter, we call them UDO-SW, UDO-NE, and UDO-SE where UDO = Ultra Diffuse Object, SW = south west, NE = north west, and SE = south east; note that UDO-SE was already found in the SDSS Stripe 82 data. Among them, both UDO-NE and UDO-SW appear to show a loop or stream structure around the main body of NGC 1068, providing evidence for the physical connection to NGC 1068. We consider that UDO-SE may be a tidal dwarf galaxy. We also find another UDO-like object that is 2 magnitudes fainter and smaller by a factor of 3 to 5 than those of the three UDOs. This object may belong to a class of low surface brightness galaxy. Since this object is located along the line connecting UDO-NE and UDO-SW, it is suggested that this object is related to the past interaction event that formed the loop by UDO-NE and UDO-SW, thus implying the physical connection to NGC 1068. Another newly-discovered feature is an asymmetric outer one-arm structure emanated from the western edge of the outermost disk of NGC 1068 together with a ripple-like structure at the opposite side. These structures are expected to arise in a late phase of a minor merger according to published numerical simulations of minor mergers. All these lines of evidence show that NGC 1068 experienced a minor merger several billions years ago. We then discuss the minor-merger driven triggering of nuclear activity in the case of NGC 1068.

Key words: galaxies: Seyfert — galaxies: individual (NGC 1068) — galaxies: dwarf — galaxies: structure — galaxies: interactions

1 Introduction

NGC 1068 is one of the archetypical Seyfert galaxies in the nearby Universe (Seyfert 1943) and belongs to a class of active galactic nuclei (AGNs). Since the majority of Seyfert galaxies

are located in the nearby Universe, many multi-wavelength observations have been made to date. Among such Seyfert galaxies, much attention has been paid to NGC 1068 because this galaxy plays an important role for a unified model of AGNs (Antonucci & Miller 1985; see for a review, Urry & Padovani 1995).

* Based on data collected at Subaru Telescope, which is operated by the National Astronomical Observatory of Japan.

Since luminous AGNs like quasars show morphological and dynamical evidence for major mergers between or among galaxies, it has been widely accepted that they are triggered by major mergers (Sanders et al. 1988; Taniguchi & Shioya 1998; Hopkins et al. 2008). On the other hand, most Seyfert galaxies appear to be ordinary-looking spiral galaxies (Malkan et al. 1998). Indeed, NGC 1068 is classified as a symmetric spiral galaxy without any morphological disturbance (de Vaucouleurs et al. 1991). However, taking all available observational properties into account, Taniguchi (1999) proposed that the Seyfert activity is triggered by a past merger with a satellite galaxy; i.e., a minor merger (see also Taniguchi 2013, Furuya & Taniguchi 2016 and references therein).

It is noted that morphological evidence for major mergers can be easily obtained because tidal remnants are prominent in most cases and double nuclei can also be seen in some cases. Meanwhile, it has been thought that it is generally difficult to find firm morphological evidence for minor mergers because their dynamical effect on the host galaxy is weak and smeared out during several rotations of the galaxy (e.g., Ji et al. 2014; Khan et al. 2012). Optical images obtained by the Sloan Digital Sky Survey (hereafter SDSS) have been often used to study morphological studies of nearby galaxies because its wide-field sky coverage and homogeneity (e.g., Fukugita et al. 2007; Willett et al. 2013, and references therein). However, the survey depth of SDSS is not deep enough (~ 25 mag arcsec $^{-2}$) to investigate faint structures in outer parts of many galaxies. Indeed, the Stripe 82 data, 2 magnitude deeper than the original SDSS, reveal such faint outer structure, providing morphological evidence for minor and/or major mergers for a sample of ordinary-looking galaxies (Schawinski et al. 2010; Willett et al. 2013). Several faint tidal features have also been found around galaxies in previous studies at 26 to 29 mag arcsec $^{-2}$ level (Martínez-Delgado et al. 2008, 2010, 2012, 2015; Chonis et al. 2011; Miskolczi et al. 2011; Duc et al. 2014, 2015). Therefore, although most Seyfert galaxies show little evidence for minor mergers, it seems worthwhile to re-visit their optical morphology by using much deeper optical images (e.g., Smirnova et al. 2010).

Here, we present our discovery of faint outer structures around the main body of NGC 1068 based on the data obtained with Hyper Suprime-Cam (hereafter HSC; Miyazaki et al. 2012) and Suprime-Cam (Miyazaki et al. 2002) on the 8.2 m Subaru Telescope. The distance toward NGC 1068, 15.9 Mpc (Kormendy & Ho 2013; we also follow their assumed WMAP 5-yr cosmology), is adopted throughout this paper; $m - M = 31.01$ and $1'' = 0.077$ kpc. We use the AB magnitude system unless otherwise noted. The single Galactic extinction value in r ($A_r = 0.08$ from the NASA Extragalactic Database; hereafter NED¹) has been applied to the photometry.

2 Observations and data analysis

2.1 Hyper Suprime-Cam observations

Our deep r -band (basically the same as the SDSS r filter, and we simply call r -band hereafter) HSC data were taken on 2016 December 25 (UTC) by the Queue observing mode (S16B-QF187; Tanaka et al.). The result of the On-Site Quality-Assurance System for HSC (the OSQA: Furusawa et al. 2017 in prep.) indicates that the transparency condition was photometric, though the seeing condition was as poor as 2 arcsec FWHM at the beginning then improved to ~ 1 arcsec.

Making a good median sky is critically important for the reliable detection of the extremely faint features around galaxies with large apparent size. To achieve this, we used a 5-step HSC-standard dither sequence for the science data acquisition² but with a fairly big dither size of 720 arcsec radius. The size of the dither circle has more than three times larger than the optical diameter of NGC 1068 ($D_{\text{maj}} \sim 7.1$ arcmin.; from NED). The wide field of view of HSC ($\phi = 1^\circ.5$) makes such big dither possible, and is a great advantage of the HSC for such nearby galaxy science.

The unit exposure was set to 80 seconds. It was chosen to balance between the efficiency and the saturation of the central region. Based on the surface photometry of NGC 1068 by Sánchez-Portal et al. (2000), we designed to allow saturation of the very central region (< 10 arcsec) around the nucleus by the setting, which is later confirmed by the actual data. In total, 2800 sec exposure was gathered with two different position angles; 0° and 90° .

Data reduction is performed using the HSC Pipeline (HscPipe ver. 4.0.5) distributed by the instrument team³. The algorithm of the pipeline is described in Bosch et al. (2017) in detail. We have applied a special sky pattern subtraction routine (Koike, M. et al. 2017, private comm.⁴) that works better for the data with large objects than the HscPipe standard procedure does. Firstly the program makes a median sky image from all exposures in each CCD after masking visible objects and normalizing the sky level. The median sky image is scaled to the sky values on each exposure data for each CCD and then subtracted. Since, at this stage, we still see some large-scale residual patterns, we have to remove these patterns in order to investigate very faint structures; i.e., we need much better object masks for apparently large objects. Therefore, the special routine tries to fit and then subtract the residual sky pattern by using the 3rd-order polynomials. Finally, the polynomial fitting for the sky in finer scale is applied by using the new more complete object masks for sky subtraction. Our observing strategy just matches to the sky-handling method used by this program. The final co-added image by the procedure is shown in figure 1.

² (https://www.naoj.org/observing/queue/HSC_QUD/node16.html)

³ see (http://hsc.mtk.nao.ac.jp/pipedoc_e/)

⁴ (http://hsc.mtk.nao.ac.jp/pipedoc_e/e_tips/skysub.html)

¹ (<http://ned.ipac.caltech.edu>)

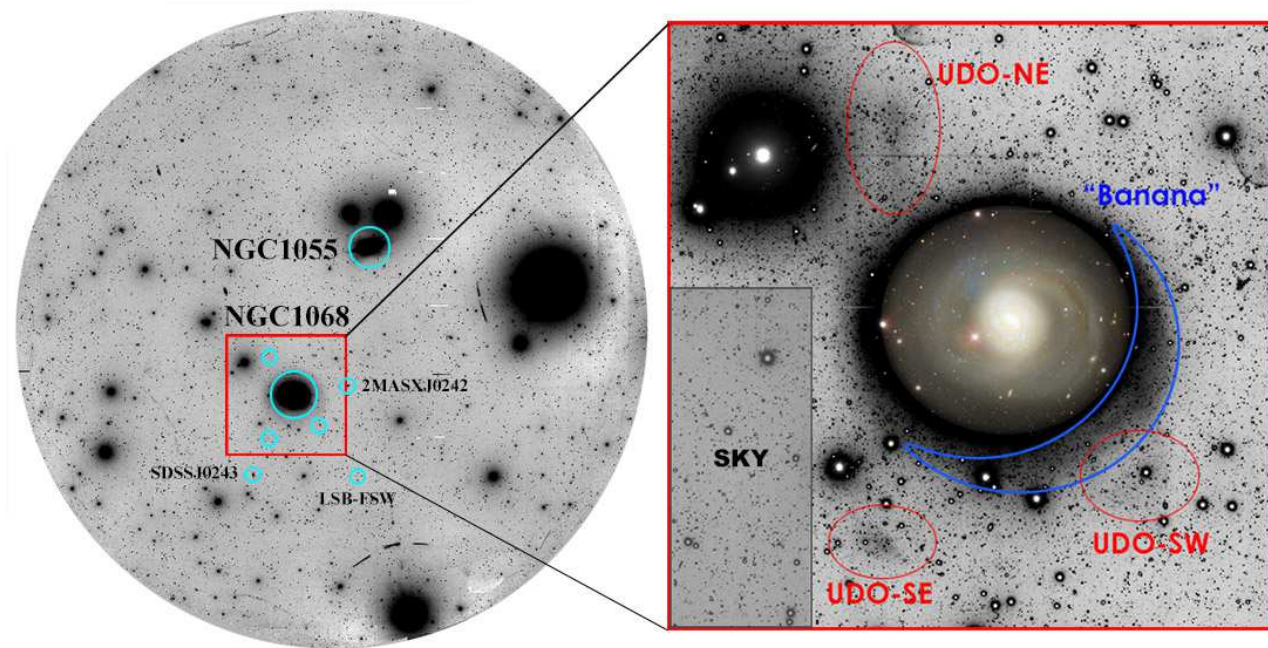


Fig. 1. (*left*) The full 3.14 deg² HSC r band image. The north is up and the east is left. The two member of the NGC 1068 group (NGC 1068 and NGC 1055), as well as the spectroscopically-confirmed member dwarf galaxies (SDSS J024310.38-001543.2 and 2MASX J02420036+0000531 labeled as SDSS J0243 and 2MASX J0242, respectively) are shown as cyan circles. Another newly-found compact diffuse dwarf “LSB-FSW” is also shown. (*right*) The 23' \times 23' cutout around NGC 1068. The three newly-discovered UDOs around NGC 1068 (see section 3) are shown with the ovals with labels. The color image of NGC 1068 from the SDSS (courtesy of Michael R. Blanton) is overlaid on the HSC data to show the detail of the inner structure. A faint outer one-arm structure is shown as blue crescent labeled as “Banana” (see section 3 as well as figures 3 and 5). The gray region labeled “SKY” is the area used for the depth measurement (see section 2.3).

The photometric and astrometric calibrations were done by the HSC Pipeline using the DR1 catalog from the Pan-STARRS1 (Chambers et al. 2016). The photometric and the astrometric accuracy measured by the pipeline (rms) is ~ 0.018 mag and $\sim 0''.03$, respectively⁵. We discuss about the depth of the HSC image in section 2.3 below.

2.2 Archived Suprime-Cam data

In addition to our own HSC imaging, we have also searched for the Subaru data archive (SMOKA: Baba et al. 2002) to see if there are any other deep imaging data for NGC 1068 available. Since our main purpose is to find evidence for very faint structures around NGC 1068, any independent observations are highly useful to confirm their presence if any. We then have found the R_c -band images of NGC 1068. The observations were made on 2014 December 17 (UTC), with 15 of 150-second exposures and 15 of 20-second exposures (in total 2550 seconds). We note that the data have become public after we submitted the HSC queue proposal for the current study.

The data reduction is the same as Yagi et al. (2017) except

⁵ In this study, we did not take the aperture correction adopted in the Pipeline into account, which makes a slight offset in the surface brightness according to the point spread function (Furusawa, H., priv. comm.). The possible offset would be < 0.1 mag at most, and does not affect our results.

for the background subtraction. As our targets in this study are widely extended objects, we first connect 10 CCDs of the same exposure and estimate a constant background of the exposure across the CCDs and subtract the value. After median coadding, we subtract the background by estimating in a mesh size of 2000 pixels (6.73 arcmin) square.

We use astrometry.net (Lang et al. 2010) for the astrometric calibration. Flux is calibrated using SDSS DR12 stars (Alam et al. 2012) with a color conversion to the Suprime-Cam system. The color conversion procedure is given in Yagi et al. (2013), and the coefficients of the color conversion are given in Yoshida et al. (2016). About 2700 stars in $18 < r < 20$ are used for the flux zero-point estimation. The rms estimated from the median of absolute deviation (MAD) is 0.04 mag. We also checked that the data were taken under good condition from the investigation of the photometric zero point of each exposure.

2.3 The depth of the data

Here we discuss about the depth of the data we use. We employ the random-aperture photometry test: we measure the fluctuation of the flux inside a fixed aperture radius for a randomly-selected blank sky area.

We firstly cut out a part of the image near NGC 1068 where

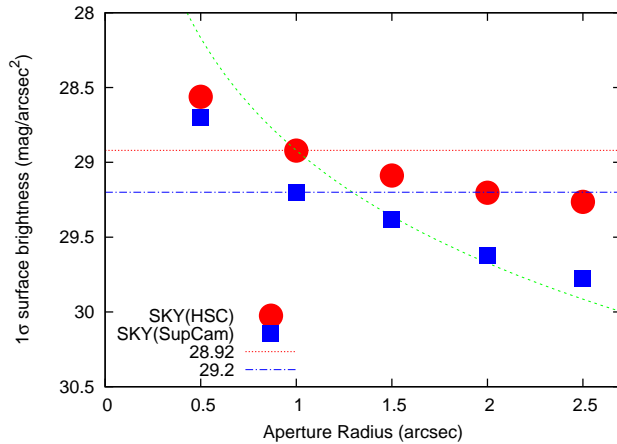


Fig. 2. The $1\text{-}\sigma$ sky fluctuation of the background of our data used. The measured $1\text{-}\sigma$ sky fluctuation in the given aperture radius is converted to the surface brightness unit. The green curve is the theoretical curve for the pure Poisson noise data in arbitrary scale.

no bright stars or galaxies exist ($5'.6 \times 12'.6$: the area labeled as "SKY" in the right panel of figure 1). After removing the residual large-scale sky pattern with 3rd-order polynomials by the IRAF `imsurfit`, we run the SExtractor (version 2.9.1; Bertin & Arnouts 1996) for the image and try to detect all the visible objects as much as possible. Using the "OBJECT" frame generated by the software, we create the object mask image. Then we generate random sky positions in the SKY image. Every time each random position is generated, we check if it is away from the areas covered by the object masks. We set the minimum acceptance distance from the masked areas to $2''.0$. We should note that larger than this acceptance separation makes the blank area for measurement extremely limited to some particular under-dense regions, as our image is very deep and most of the sky is occupied by faint objects. After generating 1000 good empty sky positions, we put aperture with the radius of $0''.5$ to $2''.5$ at each position, and measure the counts inside the apertures by the IRAF `phot`. Since the pixel scales are $0''.168 \text{ pixel}^{-1}$ (HSC) and $0''.202 \text{ pixel}^{-1}$ (Suprime-Cam), the adopted radii correspond to 3.0–14.9 pixels (HSC) and 2.5–12.4 pixels (Suprime-Cam), respectively. We then measure the standard deviation of the counts after applying a $3\text{-}\sigma$ clipping. Final results are derived by converting the counts in each aperture to mag arcsec^{-2} unit. We do the same procedure to both the HSC and the Suprime-Cam data, using the same sky region defined in the right panel of figure 1.

In figure 2 we show the $1\text{-}\sigma$ level of the sky fluctuation as a function of the aperture radius (in r band for HSC, while R_c -band in Suprime-Cam). The depth at the $1''$ -radius aperture for the HSC data is $28.9 \text{ mag arcsec}^{-2}$, while it is $29.2 \text{ mag arcsec}^{-2}$ for Suprime-Cam data. If we assume the color of the typical galaxy ($r - R_c \sim 0.05$ to 0.1 , based on the filter functions

available on the Subaru website⁶ and the galaxy SED models by Coleman et al. 1980), the Suprime-Cam data is about 0.3 mag deeper than the HSC data, though the exposure time is similar. There are a few possible reasons for this. Firstly, the seeing was quite poor ($\sim 2''$) at the first block of the data acquisition of HSC. Slower growth of the depth for HSC compared to the Suprime-Cam data points suggests that the blank sky region is actually affected by faint objects below the detection threshold. Secondly, our HSC data were taken in late 2016, just around the period when a significant degradation of the reflectivity of the primary mirror was found⁷. Thirdly, a part of (5 frames or 15%) our HSC data was taken at the elevation somewhat lower (40 to 43 degrees), though the other 85% was take at the similar elevation (60 to 69 degrees) to the Suprime-Cam data (66 to 70 degrees). The effect of the atmospheric extinction for HSC data in this study, however, should be negligibly small, as we confirmed that our data were taken under the photometric condition via our on-site quality assessment tool as well as several meteorology data of the Maunakea Observatories.

3 Results

3.1 A brief summary of our findings

The main purpose of our study is to see if there are any signatures of past interaction/mergers which may have led the current AGN activity observed in NGC 1068. As the dynamical timescale of the outer region of galaxies could extend as long as several Gyrs (e.g., Ji et al. 2014; Martínez-Delgado et al. 2008), we may expect to see, if any, remnants of such a past dynamical perturbation event.

Based on our deep HSC image, we have identified six objects summarized in table 1. Among them, three are very faint objects, being similar to ultra diffuse galaxies (UDGs) found in galaxy cluster environments (e.g., van Dokkum et al. 2015a; Koda et al. 2015; Yagi et al. 2016). Since all these are close to the main body of NGC 1068 (their projected distance from NGC 1068 are less than 45 kpc; see table 3), they are considered to be associated with NGC 1068. Their central surface brightness is fainter than $26 \text{ mag arcsec}^{-2}$ (r band) and the effective radius of these galaxies are larger than 1.5 kpc. Assuming that $g - r$ color is not extremely red ($g - r < 1.5$: note that the typical $g - r$ color of galaxies is $g - r < 0.77$; Fukugita et al. 1995), we find that these three objects satisfy the criteria for the UDGs (van Dokkum et al. 2015a). Taking account of this similarity, we call them UDO-SW, UDO-NE, and UDO-SE where UDO = Ultra Diffuse Object, SW = southwest, NE = northwest, and SE = southeast; note that UDO-SE was al-

⁶ (<https://www.naoj.org/>)

⁷ This was given in the telescope status report during the Subaru Users Meeting 2016; see (<https://www.subarutelescope.org/Science/SubaruUM/SubaruUM2016/>).

ready found in the SDSS Stripe 82 data (Bakos & Trujillo 2012). These three UDOs are shown in the right panel of figure 1.

For a cross-check, we examine the archived Suprime-Cam R_c -band data, and securely identify these three UDOs. We further examine the SDSS FITS data (Abazajian et al. 2009)⁸. However, we find that they are too faint to be securely detected, though we see a hint of UDOs after heavy smoothing. Therefore, we conclude that these UDOs are real objects (see Appendix for details). It is intriguing to note that both UDO-NE and UDO-SW appear to show a loop or stream structure around the main body of NGC 1068, providing evidence for the physical connection to NGC 1068 (see section 4.1).

We also find another UDO-like object that is 2 magnitudes fainter and smaller by a factor of 2 than those of the three UDOs. This object may belong to a class of low surface brightness galaxy. We call this object, LSB-FSW (F means ‘far’). Note that this object is out of the field of views in the Suprime-Cam R_c -band data. Although it seems uncertain if this object is physically associated with NGC 1068, we assume that this object is also a member of M77 group and a possible companion galaxy. It is interesting to note that this object is located at the line connecting both UDO-NE and UDO-SW. Therefore, we suggest that this object may be a relic of the formation of the loop structure.

The other two galaxies are identified as SDSS J024310.38-001543.2 (hereafter SDSS J0243)⁹ and 2MASX J02420036+0000531 (hereafter 2MASX J0242). They are apparently normal dwarf galaxies. Since their redshifts, 0.00370 and 0.00362 (SDSS DR13), respectively, are very close to that of NGC 1068 ($z = 0.003793$, de Vaucouleurs et al. 1991), they are considered as companion galaxies of NGC 1068. The spectroscopic information of the two dwarf galaxies are given by SDSS DR13. The spectrum of SDSS J0243 shows strong $H\delta$ absorption (Lick $H\delta_A$ index $> 5.0 \text{ \AA}$) without $H\alpha$ emission. The spectral features suggest that the galaxy is a post-starburst galaxy (e.g., Goto 2005). The spectrum of 2MASX J0242 shows strong emission lines. The $[N II]/H\alpha$ and $[O III]/H\beta$ ratios indicate that the galaxy is a typical star-forming galaxy (Baldwin et al. 1981; Kewley et al. 2001; Kauffmann et al. 2003).

In addition to the above six objects near NGC 1068, we find an asymmetric outer one-arm structure in the main body of NGC 1068, emanated from the western edge of the disk of NGC 1068 through south to east, together with a ripple-like

structure at the opposite side. Since these features are not expected to be present in isolated spiral galaxies, they may provide another line of evidence for a past minor merger.

3.2 Observational properties of the UDOs and the other companion galaxies

As described above, the three UDOs appear to be associated with NGC 1068 although there is no redshift information. In order to understand what they are, it is important to investigate their structural properties in detail. It is, however, reminded that there are some difficulties in doing such analysis because of the followings. First, they are very faint. Second, since they are close to NGC 1068 itself, their light profiles may be affected by the outskirts of NGC 1068 light. Third, there are some bright stars near UDO-NE and thus the ghost by the HSC optics overlaps with it at the faintest level. Despite these difficulties, we here try to fit their light profile carefully.

We use the model galaxy fitting code GALFIT version 3.0.5 (Peng et al. 2002; Peng et al. 2010) to derive the physical parameters. We choose the single Sérsic profile (Sérsic 1968) for fit. In order to have the reliable result from the GALFIT software, the careful sky subtraction is critically important. To achieve this, we first make the catalog of all objects in the cut-out images around the dwarf galaxies on and around the faint objects using the SExtractor (version 2.9.1: Bertin & Arnouts 1996). We then use the “OBJECT” frame generated by SExtractor for the object mask, after expanding the object regions by 2–5 pixels. The object mask made by the process is also used during the GALFIT process later. We further replace the areas with the object mask with the average sky values sampled about 100 pixels around each area. However, the object mask by the process does not include the UDO because it is so diffuse. We then replace the area around the UDO with a sky surface using the IRAF task `imedit`. Here we pay a special attention so that the profile of the interpolated sky surface is smoothly connected to the area outside. The object-eliminated frame by the process is then used for the sky pattern fitting by the two-dimensional spline function (3 terms) by the IRAF task `imsurfit`. The fitted sky surface is finally subtracted from the original cut-out images and processed by GALFIT. As the sky region is actually the outer profile of NGC 1068 and/or the halo of the nearby bright stars for UDO-NE and UDO-SW, this is the critical process for GALFIT to work properly (see below).

The basic properties measured or calculated by GALFIT for the six identified objects are summarized in table 2. The size of the detected objects is measured by using the isophote at $28.7 \text{ mag arcsec}^{-2}$ (which corresponds to $\sim 1\sigma$ surface brightness level with a $1''$ -diameter aperture) after applying the $5 \times 5 \text{ pix}^2$ boxcar smoothing to the data to suppress the noise. The residual image after subtracting the best-fit model for each object is

⁸ We used the data from both DR7 (SDSS-II final release (<http://cas.sdss.org/dr7/en/>)) and the DR12 (SDSS-III final release (<https://dr12.sdss.org/>)), because the background pattern of the UDO-SE field in the DR7 is nicer than the DR12, while the DR12 image is deeper.

⁹ We note that there are three IDs on the position of the object in the NED (others are SDSS J024310.55-001546.1 and SDSS J024310.39-001543.8). According to the SDSS Sky Server, the coordinate of the referred object better refers to the position of the object.

Table 1. Summary of the identified structures around NGC 1068

Name	Note 1	Note 2	Redshift (z)
UDO-NE	Newly discovered	A part of loop?	—
UDO-SW	Newly discovered	A part of loop?	—
UDO-SE	Bakos & Trujillo (2012)	—	—
LSB-FSW	Newly discovered	—	—
SDSS J0243	SDSS DR13	Star forming	0.00370
2MASX J0242	SDSS DR13	Post starburst	0.00362
Banana	Newly discovered	Asymmetric one arm emanated from the western edge	—
Ripple	Newly discovered	Eastern side of the outer disk	—

Note: the “ripple” and “banana” structures we claim discovery in this work can actually be visible in a few very high-quality public images posted on websites. A good examples is the one by Adam Block at the Mount Lemmon Observatory (<http://www.messier-objects.com/messier-77-cetus-a/>).

shown in the second row of figure 3. Because the objects are widely extended, we do not use automatic estimation of the sky level by GALFIT but explicitly give 0 for the sky level after carefully subtracting the sky component.

The estimate of the physical parameters (Sérsic index, r_e etc.) by GALFIT tends to be quite sensitive to the error of the sky background level (e.g., Häußler et al. 2007). As the errors estimated by GALFIT do not work to estimate the uncertainty introduced by the error of the sky background level, we simulate how the output of parameters by GALFIT changes with the error in the sky background level. We conservatively set the range of the error in the background level as $\pm 0.1\sigma$ of the sky noise. The range of the change on each parameter is given in table 2.

3.3 Distorted outer structures of NGC 1068

It is known that the disk structure of NGC 1068 at high surface-brightness level is quite symmetric. Its two spiral arms with the outer ring structure do not show any non-axisymmetric signature. At a first glance, one may consider that NGC 1068 is a spiral galaxy without any sign of galaxy interaction (Holwerda et al. 2014). However, any signatures of past dynamical disturbance is often found at faint outer envelope regions of galaxies (e.g., Martínez-Delgado et al. 2010). Therefore, in order to see such signatures, it is necessary to investigate NGC 1068 at very faint brightness levels.

As shown in the right panel of figure 1, there is an evident one-arm structure at the south-west of the disk: we call this “Banana”. In order to see this structure more clearly, we here employ the unsharp-masking technique to enhance the contrast.

To do this, we first detect all the foreground/background (compact) objects in the image using the SExtractor and eliminate them using the adjacent average count around the detected objects (“cleaned image”). For more complete detection of objects on the disk part of NGC 1068, we first apply large median filter (21 pix by 21 pix) to the data and subtract it from the original. This helps detection of compact source on significant part of the disk. After interpolation is done, we then smoothed it

using the Gaussian kernel ($\sigma = 50$ pixels) after 5 by 5 block-averaging the data to reduce the image size. In order to avoid having too strong fake negative features, we multiply 0.7 to the smoothed image. Then it is subtracted from the 5×5 block-averaged version of the cleaned image.

The result is shown in figure 4. It is clearly shown that there is a clear dip between the Banana structure and the NGC 1068 main disk. Since this dip is actually seen in the image even before the contrast enhancement, this is not due to the artificial effect of the unsharp-masking technique. In figure 5 we also show the radial surface brightness profile of a part of the NGC 1068 disk (before unsharp-masking) that includes the Banana region. A narrow rectangular region (35-pixel width) from the center of NGC 1068 toward southwest direction (position angle = -135°) is cut out and used for this analysis. The exponential disk is well fit at the high surface-brightness area of the disk (from $200''$ to $280''$ area in red), and with a clear discontinuity (labeled as “dip”) the flux excess at the Banana region is clearly shown.

Another notable feature seen in the unsharp-masked image is a ripple-like structure at the opposite side of the one-arm Banana structure (it is labeled as “Ripple” in figure 4). Since they appear at opposite positions, one may consider that they are not physically related. However, such a pair of unusual structures can be seen in minor merger simulations that reproduce the ring-like features discovered in our Milky Way (Kazantzidis et al. 2008; Purcell et al. 2011). This reinforces that NGC 1068 experienced a past minor merger in its life. We will discuss this issue more in the next section.

4 Discussion

4.1 The nature of the NGC 1068 UDOs

The three UDOs all have very small Sérsic index (n), while they have similarly large effective radius as the cluster UDGs (van Dokkum et al. 2015a; Koda et al. 2015; Yagi et al. 2016). This is a significant difference from the UDGs found in cluster environment. We here compare some physical parameters of

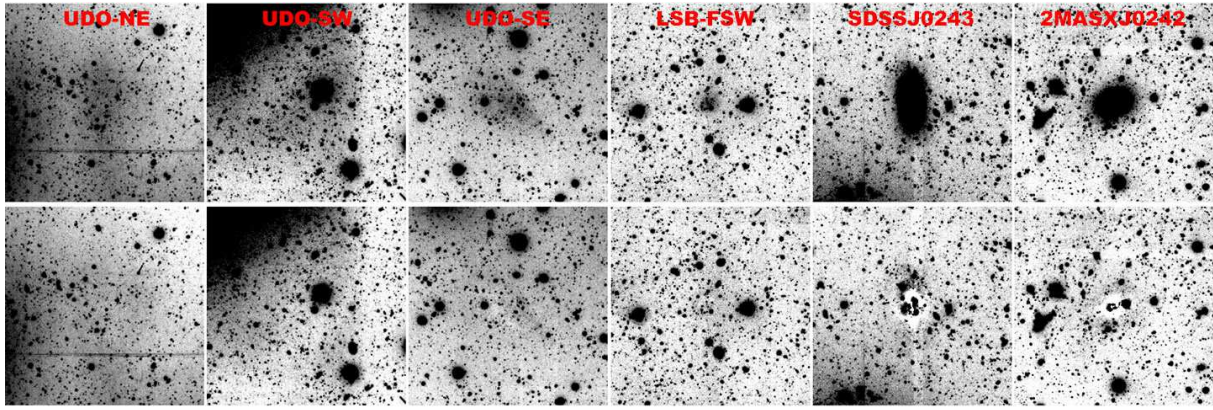


Fig. 3. The newly-discovered ultra-diffuse objects (from left to right, UDO-NE, UDO-SW, UDO-SE), as well as a candidate faint companion dwarf (LSB-FSW), and the known two bright companion dwarf galaxies (SDSS J024310.38-001543.2 and 2MASX J02420036+0000531) are shown at the top. The images in the second row are after subtracting the best-fit model galaxy by GALFIT. Each cutout has $4'.48$ on a side.

Table 2. The structural properties of the six identified objects around NGC 1068

Name	R.A. J2000.0	Dec. J2000.0	distance arcmin.	r mag	μ_0 mag arcsec $^{-2}$	Size arcmin.	Sérsic n	r_e arcsec.	b/a	$\langle\mu(r_e)\rangle$ mag arcsec $^{-2}$
UDO-NE	02 ^h 42 ^m 57 ^s .65	+00°06′18″.5	8.58	17.3 ± 0.4	26.97 ± 0.2	2.7 × 1.2	0.40 ^{0.31} _{0.66}	58 ⁴⁸ ₇₇	0.44	28.1 ^{27.7} _{28.8}
UDO-SW	02 ^h 42 ^m 21 ^s .57	−00°06′45″.2	7.52	17.5 ± 0.5	27.02 ± 0.3	3.3 × 1.4	0.39 ^{0.26} _{0.83}	70 ⁶⁰ ₁₀₆	0.53	28.7 ^{28.4} _{29.6}
UDO-SE	02 ^h 43 ^m 00 ^s .48	−00°09′00″.1	9.48	17.6 ± 0.1	26.40 ± 0.05	1.8 × 1.0	0.38 ^{0.31} _{0.89}	38 ³⁴ ₅₄	0.59	27.5 ^{27.3} _{28.3}
LSB-FSW	02 ^h 41 ^m 53 ^s .51	−00°15′49″.3	19.11	19.4 ± 0.1	26.19 ± 0.03	0.7 × 0.6	0.45 ^{0.34} _{0.84}	12.2 ^{10.8} _{17.5}	0.91	26.9 ^{26.6} _{27.8}
SDSSJ0243	02 ^h 43 ^m 10 ^s .46	−00°15′44″.4	16.69	15.40 ± 0.05	21.92 ± 0.02	2.0 × 1.1	1.12 ^{1.08} _{1.18}	17.4 ^{17.0} _{18.0}	0.54	23.54 ^{23.50} _{23.60}
2MASXJ0242	02 ^h 42 ^m 00 ^s .38	+00°00′52″.3	10.22	15.46 ± 0.05	20.24 ± 0.02	1.4 × 1.2	2.02 ^{1.94} _{2.12}	8.9 ^{8.7} _{9.2}	0.67	22.22 ^{22.17} _{22.27}

Notes: SDSS J0243 and 2MASX J0242 refer to SDSS J024310.38-001543.2 and 2MASX J02420036+0000531, respectively. The distance refers to the projected distance from the center of NGC 1068. The r mag and the central surface brightness μ_0 are the observed value (in AB). The size of the detected objects is measured in the 28.7 mag arcsec $^{-2}$ isophote. The effective surface brightness ($\langle\mu(r_e)\rangle$) is the average surface brightness within the radius of r_e . The range of uncertainties of the physical parameters by GALFIT is estimated by artificially changing the sky level by $\pm 0.1\sigma$. The superscript and subscript numbers refer to the value for the case where the sky estimate is wrong by $+0.1\sigma$ and -0.1σ , respectively.

our NGC 1068 UDOs with those of other similar objects from the literature. To do this, the observed values in table 2 are converted to the physical values in table 3, adopting the distance of 15.9 Mpc and assumed all the dwarfs listed are at the same distance.

In figure 6, we show the following two diagrams; the absolute magnitude versus effective radius (upper panel), and the Sérsic index versus $\langle\mu(r_e)\rangle$, the average surface brightness within the effective radius (lower panel). In order to compare the properties of both the NGC 1068 UDOs and the other companions, we also plot the data for the normal dwarf galaxies in the Virgo (Gavazzi et al. 2005) and the Coma (Mobasher et al. 2001; Komiyama et al. 2002) clusters, the UDGs and their analogs in the Coma cluster from Yagi et al. (2016) as well as their UDG subsample originally detected in g -band by van Dokkum et al. (2015a). For the Yagi et al. (2016) sample, we use the values from the 1-component Sérsic fit given in their table 4. Here we convert our photometry values and values from the literature to R_c in the AB system ($R_{c,AB} - R_{c,Vega} = 0.22$) using the color of the elliptical galaxies from the Coleman et al. (1980) model SEDs calculated by us ($B_{Vega} - R_{c,Vega} = 1.51$ and $r'_{AB} - R_{c,AB} = 0.07$). For the $m - M$ conversion to the

Coma and the Virgo clusters, we use the values 35.04 and 30.70 (from NED; here the WMAP 5-yr cosmology is adopted), respectively.

The upper panel of figure 6 shows that our NGC 1068 UDOs have similarly large size to the UDGs discovered by van Dokkum et al. (2015a) and Yagi et al. (2016), while they are roughly 1–2 mag fainter. On the other hand, the three companions (2MASX J0242, SDSS J0243 and LSB-FSW) are located in the sequence of the ‘normal’ dwarfs with a small effective radius. This demonstrates that the NGC 1068 UDOs are structurally different populations from these ‘normal’ dwarf galaxies.

The extreme nature of the NGC 1068 UDOs is demonstrated in the lower panel of figure 6. They are distributed at the smallest extreme of the Sérsic index and the faintest end of the average surface brightness¹⁰, while the two companions lie in the sequence of a larger Sérsic index for brighter surface brightness, made by the Virgo normal dwarfs (Graham & Guzmán 2003). Here note that we use the distance of 15.9 Mpc for NGC 1068

¹⁰For reference, we mention that 4 UDGs around NGC 5485 reported by Merritt et al. (2016) have comparable Sérsic indices (0.3–0.7) to those of the UDOs in this study.

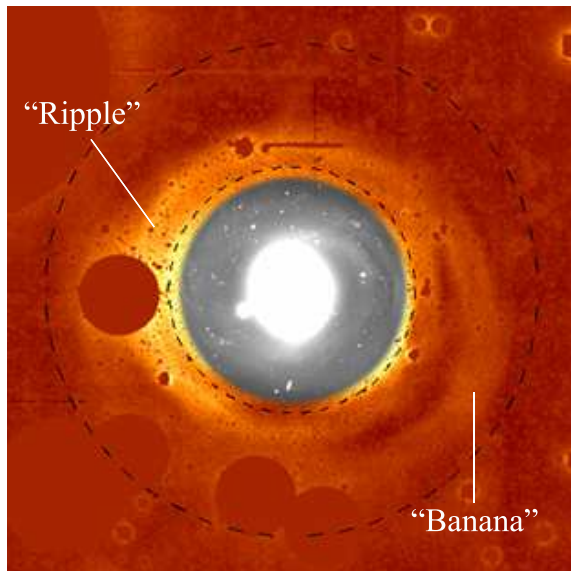


Fig. 4. The detail of the “Banana” structure and the location of the “Ripple”. The unsharp-masking contrast enhance method is applied to the HSC data after eliminating the foreground/background objects interpolated by the adjacent sky. The dashed small and large circles show the radius of $3'.4$ and $6'.8$ from the center, respectively. We also show the original HSC image of NGC 1068 inside the small circle with gray scale in shallow contrast.

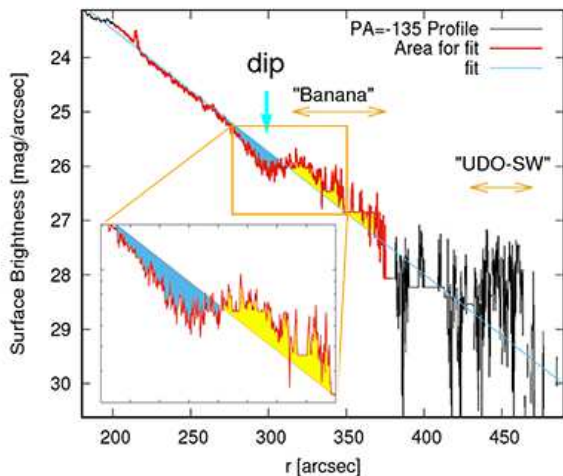


Fig. 5. Radial surface brightness profile toward the southwest direction ($PA = -135$ deg) as a function of the distance from the center of NGC 1068. The black line shows a series of the median count in 35 pixels. All foreground/background objects in the region are replaced to the adjacent counts before radial profile is made. The orange line shows the fit of the exponential disk profile, and the fitted range is shown as red points. The inset is the zoomed view of the dip & the Banana areas. The dip and the Banana region are evidently recognized. We note that the small excess flux at $r \sim 200''$ is the edge of the outer ring.

Table 3. The physical properties of the objects in table 2.

Name	distance kpc	$M(r)$ mag	Size kpc	r_e kpc
UDO-NE	39.70	-13.7	12.7×5.3	$4.5^{3.7}_{5.9}$
UDO-SW	34.77	-13.5	15.3×6.2	$5.4^{4.6}_{8.2}$
UDO-SE	43.86	-13.4	8.3×4.6	$2.9^{2.7}_{4.2}$
LSB-FSW	88.36	-11.6	3.0×2.8	$1.0^{0.9}_{1.5}$
SDSS J0243	77.19	-15.61	9.0×5.1	$1.31^{1.28}_{1.34}$
2MASX J0242	47.28	-15.55	6.6×5.3	$0.69^{0.68}_{0.71}$

Notes: see notes in table 2 for the object names and the uncertainty range in r_e . We use the distance of 15.9 Mpc for all the objects (see text).

from its recession velocity (Kormendy & Ho 2013). If we take a shorter distance of 10.3 ± 3 Mpc from the measurements by Tully-Fisher relation (from NED), the absolute magnitudes of the UDOs are estimated as ~ 1 magnitude fainter and the scale length become 64% smaller. Moreover, the parameters used in the lower panel, Sérsic n and $\langle \mu(r_e) \rangle$, are unaffected by the change of the distance. Thus, the extreme nature of the UDOs presented here in figure 6 basically does not change. It is also interesting to note that LSB-FSW also shares the same property as those of the NGC 1068 UDOs, while its physical size is 3 to 5 times smaller. The small Sérsic index indicates a flat-top stellar distribution (Graham & Driver 2005). Such a less centrally-concentrated stellar distribution implies that the UDOs around NGC 1068 may have a shallower gravitational potential and thus lesser content of dark matter than the UDGs found in clusters (van Dokkum et al. 2015b; van Dokkum et al. 2016).

The observed extreme nature of the NGC 1068 UDOs suggests that their origin is different from that of cluster UDGs. If the three UDOs are remnants of a past minor merger, one possibility is that they are tidally induced dwarf galaxies (‘tidal dwarf’ galaxy; Barnes & Hernquist 1992). In fact, UDO-SE appears to be located at the end of the Banana structure. On the other hand, as noted before, both UDO-NE and UDO-SW may consist of a loop (or stream) structure around NGC 1068 because both UDO-NE and UDO-SW show a sign of connection to NGC 1068. In order to see their morphological property in more detail, we make contrast-enhanced images of these UDOs. The results are shown in figure 7. Here we use the Suprime-Cam data for UDO-NE while the HSC data for UDO-SW taking account of their relative image quality.

If this loop interpretation is correct, its physical size is 74.6 kpc in diameter, with the projected ellipticity (b/a) of 0.264. If the loop has the circular shape, the viewing angle toward the loop is estimated as 15.3 degrees. Assuming that the dynamical mass of NGC 1068 within the 74.6 kpc sphere is $3 \times 10^{11} M_\odot$ (Dickel & Rood 1978, converted to the cosmology we adopted here), the size of the loop indicates the orbital period of 1.2 Gyr. In order to turn the tidal debris into the loop, it may require several orbital timescale as suggested by Martínez-Delgado et

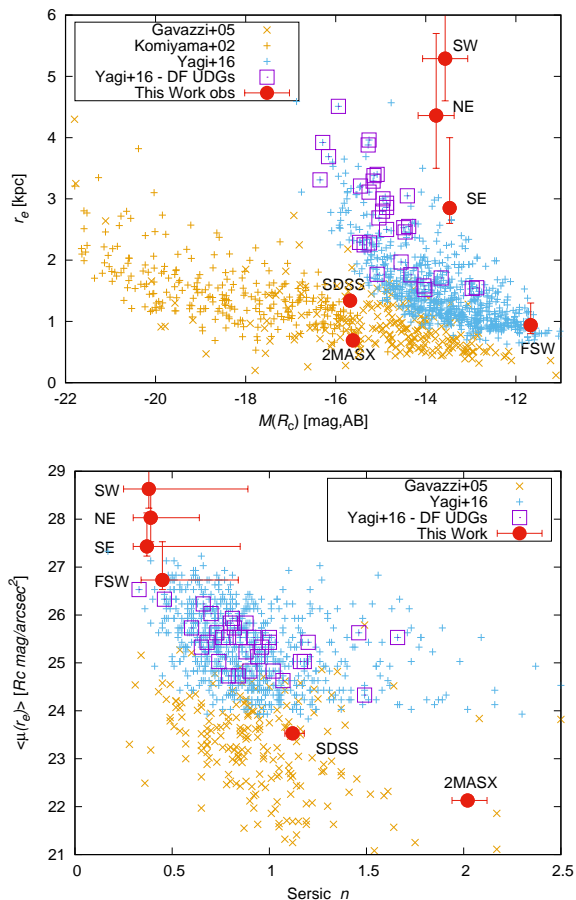


Fig. 6. (Top) Comparison of the objects found around the NGC 1068 with some similar objects in the literature in the absolute magnitude versus effective radius diagram. (Bottom) The same figure for the Sérsic index versus $\langle \mu(r_e) \rangle$ (average surface brightness within the effective radius). Note that FSW, SDSS, and 2MASX are LSB-FSW, SDSS J0242, and 2MASX J0242, respectively.

al. (2008). Thus, the first encounter that made the loop could be more than 5 Gyr ago. The core (or nucleus) of the satellite might have already merged into the NGC 1068 due to the dynamical friction during the interaction with the disk.

We further estimate the total magnitude of the loop. First, we assume the geometry of the loop is a torus whose major and minor radii are 74.6 kpc and 3.5 kpc, respectively. The projected area of the loop is 3.5×10^5 arcsec². Since some part of the loop is not seen even in our deep data, we roughly assume that the mean surface brightness of the loop would be ~ 29 mag arcsec⁻². Then, the total apparent magnitude of the loop is about 15 mag, and the absolute magnitude is about -16 mag. Though the error might be large, the absolute magnitude is comparable to those of normal dwarf galaxies, and the scenario would be valid that the loop is a remnant of an infalled satellite. The above absolute magnitude corresponds to the luminosity of $L \sim 2 \times 10^8 L_\odot$, where we assume that the absolute magnitude of the Sun in r-band is 4.64 (Blanton & Roweis 2007). Given the

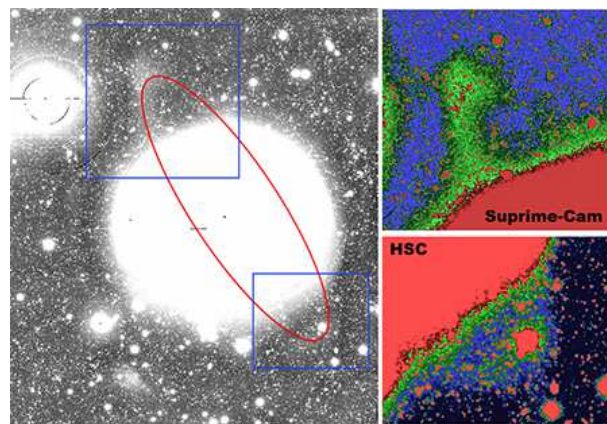


Fig. 7. A possible loop structure which connects UDO-NE and UDO-SW. A contrast-enhanced image for UDO-NE (upper right) is from the Suprime-Cam data, while that for UDO-SW is from the HSC images.

mass-to-luminosity ratio, $M/L \sim 10$ (Robert & Haynes 1994), we obtain the mass of $M \sim 2 \times 10^9 M_\odot$. Since the nucleated fraction in galaxies is higher for larger-mass galaxies (Miller et al. 2015), it is expected that the infalled satellite would have a supermassive black hole (hereafter SMBH) with the mass $M_{\text{SMBH}} \sim 2 \times 10^6 M_\odot$, given the stellar to SMBH mass ratio of 1000 (e.g., Kormendy & Ho 2013). Here, it is reminded that one of the satellite galaxies of M 31, M 32, has the stellar mass $M \sim 3 \times 10^9 M_\odot$ and $M_{\text{SMBH}} \sim 3 \times 10^6 M_\odot$ (Kormendy & Ho 2013). We may imagine that M 32 will merge into M 31 and then we will see a similar loop structure around M 31 several Gyrs after.

Here, let us re-visit UDO-SE. Although it may be a tidal dwarf galaxy, we cannot exclude a possibility that it is an isolated faint dwarf galaxy. If this is the case, we can set constraints on its mass. UDO-SE lies at projected distance of 43.9 kpc. Assuming that the total mass of NGC 1068 is $\sim 3 \times 10^{11} M_\odot$ within the 43.9 kpc sphere, and the self gravity of UDO-SE maintains its shape at least in < 2 kpc, the mass of UDO-SE in 2 kpc radius should be larger than $8.5 \times 10^7 M_\odot$ (Binney & Tremine 1987). As the luminosity of UDO-SE is $\sim 1.6 \times 10^7 L_\odot$ in r band, the M/L of UDO-SE is $\gtrsim 5.3$, which is similar to the nearby normal dwarf and the LSB galaxies (average ~ 7.7 ; Swaters et al. 2011). Therefore, UDO-SE is probably not a simple tidal debris without dark matter, but seems to be a normal dwarf galaxy with its own dark-matter halo. The stretched shape of the UDO-SE, however, suggests that it is currently in a disrupting phase. If this is the case, the galaxy passed near NGC 1068 (hence stronger tidal force) in the recent past. Or, the M/L ratio could actually be smaller than the normal dwarfs. If the close encounter would have stimulated the star-formation on UDO-SE, the lower M/L may be expected. A future color information for this object is necessary to fix this issue.

4.2 Possible origins of the loop, UDOs, and warped disk

As we have already discussed, UDO-SW and UDO-NE may be a part of the loop. The most likely origin of this loop is that the stellar envelope of a satellite dwarf galaxy has been stripped by the interaction with NGC 1068. The best example of such a tidally liberated loop is seen around the edge-on spiral galaxy NGC 5907 (Martínez-Delgado et al. 2008). We show the possible interpretation of the single, circular loop in figure 7. However, the actual loop structure may be more complex as seen in the case of NGC 5907. In this respect, we cannot exclude a possibility that UDO-SE is a remnant that was made during the process of the loop formation.

If there was the past interaction event that has led the formation of the loop, one may consider that the “Banana” structure found at the outer disk (section 3.3) could also be the fossil record of the event. Indeed, the appearance of the NGC 1068 outer disk is strikingly similar to the result of a minor-merger simulation presented in Kazantzidis et al. (2008). They claimed that the duration of such outer one-arm or ripple structures are not short-lived but could last as long as ~ 4 Gyrs after the minor merger. A similar simulation was also made by Purcell et al. (2011). They explained the origin of a ring or ripple structure on a smooth disk by the infall of a single satellite galaxy. It is interesting to speculate that the core of the satellite galaxy may have sunk into the center of NGC 1068 subsequently and have turned on the AGN activity as we see today (Taniguchi 1999). We will discuss about this in the next section.

4.3 Comments on a nucleated minor merger for the triggering AGN

NGC 1068 is an ordinary looking spiral galaxy although it belongs to the M 77 (= NGC 1068) group of galaxies together with NGC 1055, and so on (Huchra & Geller 1982). Its morphology is classified as (R)SA(rs)b (de Vaucouleurs et al. 1991). Hence, it is generally thought that NGC 1068 can be regarded as an isolated galaxy that experienced no past minor merger. However, several lines of evidence for a past minor merger in NGC 1068 have been accumulated to date.

4.3.1 Supporting evidence for a minor merger

(1) Kinematically decoupled two stellar systems in the nuclear region: García-Lorenzo et al. (1997) made spectroscopic investigation of the central $20 \text{ arcsec} \times 40 \text{ arcsec}$ region of NGC 1068 using the Ca II triplet line, and identified the off-centering of the rotation axis between the inner ($r < 3 \text{ pc}$) and the outer ($r > 5 \text{ pc}$) regions. This result indicates the presence of non-symmetric gravitational potential in the nuclear region. The most plausible interpretation is that this non-symmetric property is attributed to a past minor merger. It is here reminded

that the satellite galaxy should have a nucleus (i.e., an SMBH) in its center. Otherwise, the minor merger cannot affect the nuclear stellar dynamics in its host galaxy (see 4.3.2).

(2) The narrow line region inclined from the rotational axis of the main disk: The narrow line region (NLR) is an ionized gas-cloud system with a scale of 100 pc to 1 kpc, and is one of important characteristics of AGNs. The NLR is photoionized by the central engine although shock heating also works to some extent. Since the central engine is surrounded by a molecular/dusty torus with a typical radius is 0.1 pc to 10 pc (e.g., Taniguchi & Murayama 1998), ionizing photons from the central engine are generally collimated by the torus. In fact, it is often observed that the NLR shows a biconical structure (Schmitt & Kinney 1996). This property is also observed in NGC 1068. If the gas accretion onto the SMBH occurs taking an orbit in the plane of the main disk of NGC 1068, the torus would locate in the main disk plane, and thus the biconical NLR should be observed along the rotational axis of the main disk. However, the NLR of NGC 1068 is highly inclined from the rotational axis (~ 50 degree; Cecil et al. 2002). This means that the torus plane itself is inclined from the main disk. We note that such a property is often observed in a number of Seyfert galaxies, in particular, type-2 Seyferts (Schmitt & Kinney 1996). This random nature of NLRs in Seyferts favors the minor-merger driven triggering of AGNs (Taniguchi 1999; Taniguchi 2013).

(3) The edge-on view molecular/dusty torus in the central 0.1 pc region: The molecular/dusty torus in NGC 1068 has been probed by using the water maser emission at 22 GHz (Gallimore et al. 1996, 2001, 2004; Greenhill et al. 1996); its inner and outer radii are 0.4 pc and 0.7 pc, respectively (Greenhill et al. 1996). The observed rotation curve of H₂O maser emission provides a nuclear mass within a radius of 0.7 pc, $\sim 1 \times 10^7 M_{\odot}$ at the distance of NGC 1068, 15 Mpc (Greenhill et al. 1996). Based on this observation, Lodato & Bertin (2003) obtained the mass of the central SMBH as $8 \times 10^6 M_{\odot}$ at the distance of NGC 1068, 14.4 Mpc. At the distance adopted in this paper, 15.9 Mpc, the nuclear mass within a radius of 0.7 pc, $\sim 1 \times 10^7 M_{\odot}$. Since the mass of the putative secondary SMBH supplied by the merging satellite galaxy is a few $\times 10^6 M_{\odot}$ at most, its contribution to the nuclear mass is acceptably small.

The observed torus is the edge-on view while the main disk of NGC 1068 is not viewed as so; the optical axial ratio of NGC 1068, $b/a = 0.89$ gives a viewing angle $i = 63^{\circ}$, being far from the edge-on view ($a = 540.0 \text{ arcsec}$ and $b = 480.6 \text{ arcsec}$ are given in the NED). The edge-on view nature of the torus explains why the central engine and the broad line region cannot be seen because they are hidden by the optically-thick dusty torus while they can be seen in the polarized light through the electron scattering (Antonucci & Miller 1985). Here, an important point is that the torus is kinematically decoupled from the main disk. If the material of the torus could be supplied from

accreting gas clouds in the nuclear disk region of NGC 1068, the torus would be located in the main disk plane. On the other hand, the minor merger scenario naturally explains this kinematically decoupled property because minor mergers occur by taking a randomly oriented orbit rather than the coplanar orbit.

4.3.2 On the importance of a nucleated minor merger

Minor mergers can be classified into the following two types. One is nucleated minor mergers in which a nucleated satellite galaxy merges into its host galaxy. The other one is non-nucleated minor mergers in which a non-nucleated satellite galaxy merges into its host galaxy. Here, the term of “nucleated” means that a satellite galaxy has a nucleus (a SMBH). In the case of non-nucleated minor mergers, stars in a satellite galaxy are scattered into the galactic disk of its host galaxy during the course of the minor merging process (e.g., Khan et al. 2012). On the other hand, in the case of nucleated minor mergers, its nucleus (a SMBH) can migrate into the nuclear region of the host galaxy while most stars in the satellite galaxy are also scattered into the host disk. Therefore, this type of minor mergers can trigger the nuclear activity in the host nucleus because the dynamical effect caused by the sinking secondary nucleus leads to the efficient gas fueling onto the primary nucleus. It is noted that intense circumnuclear ($r \sim 100$ pc) star formation is also triggered by the dynamical effect of the secondary nucleus before going into the very nuclear region (Taniguchi & Wada 1996).

Here, let us go back to the case of NGC 1068. It has been recognized that NGC 1068 has a luminous circumnuclear starburst (CNSB) region that shows a ring-like morphology at a radius of $r \sim 1$ kpc with a luminosity of $L_{\text{CNSB}} \sim 10^{11} L_{\odot}$ (Telesco et al. 1984; see also Taniguchi 1997). If NGC 1068 is an isolated galaxy for a long time, it seems difficult to explain what mechanism causes the luminous CNSB as well as the AGN phenomenon. However, if NGC 1068 would experience a nucleated minor merger, both its CNSB and AGN phenomenon could be explained without taking account of any other physical processes because the sinking secondary SMBH causes a luminous CNSB first and then gas fueling onto the primary SMBH (Taniguchi 1997; Taniguchi 2013). Namely, during the course of a nucleated minor merger, a CNSB comes first, and then an AGN phenomenon comes later. This sequence is also proposed for major mergers (Hopkins et al. 2008). It is also noted that starburst galaxies tend to have more disturbed morphology than Seyfert galaxies (Schawinski et al. 2010), suggesting again that a circumnuclear starburst comes first and then AGN comes later.

Then, let us consider which is the case: i.e., a nucleated minor merger or not in the case of NGC 1068. First, we revisit the molecular/dusty torus probed by the water maser emission. In addition to NGC 1068, the best-studied torus is that in NGC 4258 (Miyoshi et al. 1995). However, there is a signifi-

cant difference in the dynamical properties of the tori between NGC 4258 and NGC 1068. Namely, the torus of NGC 4258 shows the Keplerian rotation while that of NGC 1068 shows non-Keplerian rotation (the velocity v is proportional to $r^{-1/3}$; Greenhill et al. 1996). Murayama & Taniguchi (1997) suggested that the non-Keplerian rotation in NGC 1068 can be attributed to the dynamical effect of a bar structure inside the torus. However, it is noted that the dynamical effect of a bar is equivalent to that of a pair of SMBHs; one is the SMBH already resided in the center of NGC 1068 while the other one is a SMBH supplied by a sinking satellite galaxy.

Another important observational evidence for the nucleated minor merger in NGC 1068 is the presence of the kinematically decoupled two stellar system in the nuclear region reported by García-Lorenzo et al. (1997). The two off-centered stellar system between the inner ($r < 3$ pc) and the outer ($r > 5$ pc) regions cannot be attributed to a non-nucleated minor merger because such a merger can never affect the stellar dynamics in the very nuclear region. The nucleated minor merger hypothesis also explains two distinct, episodic star formation events: ~ 300 Myr ago in the central 180 pc (in radius) region, and ~ 30 Myr ago in the ring at $r \simeq 100$ pc region (Storchi-Bergamini et al. 2012).

Here, we propose a hypothesis of the past history of NGC 1068. Several Gyrs ago, a nucleated satellite galaxy began to fall onto NGC 1068. The tidal force of NGC 1068 stripped stars of the satellite galaxy to create the observed loop structure. After a few orbital rotations, the satellite galaxy gradually falls onto near nuclear regions. Recently, 500 Myrs ago, the SMBH of the satellite galaxy approached to a few hundreds pc from the SMBH of NGC 1068 and ignited the central starburst; e.g., Taniguchi (1997). Then, the SMBH continues to sink into the nuclear region (i.e., < 1 pc), and finally stimulates the AGN by fueling the gas of the NGC 1068 disk. This hypothesis would be examined by future observations. The color of the UDOs would set constraints on their stellar population. Also, spectroscopic observations of the Banana, the Ripple, and the UDOs will give us kinematic information of the structures and enables us to reconstruct the whole merging history.

5 Conclusion

Minor mergers have been considered as one of triggering mechanisms of AGNs, in particular, Seyfert galaxies (Taniguchi 1999; Taniguchi 2013). Therefore, it is important to search for firm observational evidence for minor mergers in Seyfert galaxies. However, since tidal effects of minor mergers are generally weak, it has been difficult to identify convincing evidence for minor mergers in Seyfert galaxies.

In this paper, we have presented our deep optical imaging of the archetypical type 2 Seyfert galaxy, NGC 1068 (M77) carried out by using both Hyper Suprime-Cam and Suprime-

Cam on the 8.2 m Subaru Telescope where the Suprime-Cam data were taken from the SMOKA data archive. Our deep optical data has enabled us to do the census of very faint features around NGC 1068 at ~ 29 mag arcsec $^{-2}$ surface brightness level.

The main results and conclusion are as follows.

1. It is found that the three ultra diffuse objects (UDOs) appear to be associated with NGC 1068; they are called as UDO-NE, UDO-SW, and UDO-SE. Note that UDO-SE was previously identified in Bakos & Trujillo (2012) based on the SDSS Stripe 82 data.
2. The three UDOs around NGC 1068 have the following properties; i) their Sérsic indices are fairly small (< 0.5), and ii) their average effective surface brightness is very low ($\langle \mu(r_e) \rangle > 26$ mag arcsec $^{-2}$). Therefore, it is suggested that they are different populations from UDGs found in the cluster environment. A plausible idea is that they are tidally induced objects during the course of a past minor merger.
3. The detailed morphological properties of both UDO-NE and UDO-SW suggest that these two structures would make a single loop surrounding the main body of NGC 1068, being similar to those found in our Galaxy (Newberg et al. 2002), NGC 5907 (Martínez-Delgado et al. 2008), and so on. If this is the case, the two UDOs (UDO-NE and UDO-SW) is a so-called stream structure that is a tidal remnant of a merging satellite galaxy.
4. Another UDO-like object is also found at far SW. This object is ~ 2 magnitudes fainter and smaller by a factor of 3–5 than those of the three UDOs. This object may belong to a class of low surface brightness galaxy and thus we call it LSB-FSW. Since there is no redshift information, it is difficult to confirm its physical connection to NGC 1068. However, it is interesting to note that this object is located at the line connecting both UDO-NE and UDO-SW. Therefore, we suggest that this object may be a relic of the formation of the loop structure.
5. In addition to the UDOs, it is also found that an outer one-arm structure is emanated from the SW edge of the main body of NGC 1068; we call this the Banana structure. And also, a ripple-like structure is found at the opposite side of the outer disk. A plausible idea is again that they are tidally induced structures of a past minor merger.
6. All the above observational results provide evidence for a past minor merger occurred in NGC 1068 several billions years ago.

Since NGC 1068 appears to be an ordinary looking, beautiful and symmetric spiral galaxy, we tend to regard this galaxy as an isolated galaxy. Therefore, it has been often considered that the nuclear activity in NGC 1068 is not related to any merger events (García-Burillo et al. 2014, and references therein). Yet, several lines of supporting evidence for a minor merger in

NGC 1068; (a) the presence of kinematically decoupled two stellar population systems within the central several parsec region, (b) the presence of the molecular-dusty torus whose rotational axis is almost orthogonal to the main disk of NGC 1068, and (c) the nuclear radio jet axis as well as that of NLR is also highly inclined with respect to the rotational axis of the main disk. Now, together with our new discovery presented in this paper, all these properties can be reasonably interpreted as the effect of a past minor merger. Another important aspect is that a past minor merger surely affected the dynamics of central parsec region. This strongly suggests that the putative satellite galaxy merged into NGC 1068 is a nucleated satellite galaxy such as M 32 which has an SMBH with mass of $\sim 10^6 M_\odot$ (Kormendy & Ho 2013, and references therein).

Acknowledgments

We greatly appreciate the anonymous referee for his/her useful comments and suggestions that helped us to improve our paper. We thank Yutaka Komiyama for providing us their unpublished r_e catalog for Coma Dwarfs as well as his useful comments. We also thank Mikito Tanaka, and Keiichi Wada for their useful comments. We thank Hisanori Furusawa, Michitaro Koike, and the member of the HSC pipeline HelpDesk for their help for our HSC data analysis. IT thanks Fumiaki Nakata for his efforts on building the HSC data analysis environment in Subaru Observatory. We appreciate the operation staff of the Subaru Observatory for the execution of our Queue program. We would also like to thank Michael R. Blanton for providing us the SDSS color image of NGC 1068 for our figure 1. This work has made use of the SDSS database and the NASA/IPAC Extragalactic Database (NED). We also used the photometric and astrometric data from the Pan-STARRS1 Survey (PS1) database during the HSC data analysis. This work has also made use of the SMOKA archive and the computer systems at Astronomical Data Analysis Center of National Astronomical Observatory of Japan (NAOJ). This work was supported by JSPS KAKENHI Grant Number 16H02166 (YT). Finally, we wish to recognize and acknowledge the very significant cultural role and reverence that the summit of Maunakea has always had within the indigenous Hawaiian community. We are most fortunate to have the opportunity to conduct observations from this mountain.

Appendix. Possible effects of the CCD edges on the shape of the UDOs

There are some concerns about whether the shape of the UDO-SW and NE are affected by the CCD edges, because the left side of UDO-NE and right side of UDO-SW that makes up the loop are apparently aligned with the CCD columns. To see whether the morphology is affected by the CCD edges, we compare the exposure map with the morphology of the UDO-SW and NE.

We first divide 33 exposure dataset into 3 subsets, each of which contains 11 frames. We then combine the data in each subset. We do not use the last 2 of the whole 35 frames for the test, since it is better to keep the number of each subset the same. We also generate the exposure map for each. If the morphology of the UDOs are significantly different among the

subsets, or if the exposure map pattern and the outer edges of the UDO-NE and/or SW show a clear correlation, it indicates that the morphology is affected by the CCD columns.

The result is shown in figure 8. We can see that the CCD gaps as seen in the exposure map sometimes show rectilinear patterns either on the sky or on the stellar halo. However, the overall morphology of three UDOs in each subset appears to be the same as the total image in which all the 33 exposures are combined. Thus we conclude that the CCD edges does not significantly affect the overall morphology of the UDO-SW and NE. We should note that the shape of objects in the frames combined the 33 frames and all 35 frames are indistinguishable.

We also compare the morphology of each UDOs in HSC, Suprime-Cam, and the SDSS DR12 data. The result is shown in figure 9. Overall, the shapes of objects in the HSC data are fairly similar to those in the Suprime-Cam data. Although the SDSS data is shallow and largely affected by worse sky subtraction, we can see the trace of the three UDOs. Thus we conclude that their presence is real.

References

- Abazajian, K. N., Adelman-McCarthy, J. K., Agüeros, M. A. et al. 2009, *ApJS*, 182, 543
- Alam, S., Albareti, F. D., Allende Prieto, C. et al. 2015, *ApJS*, 219, 12
- Antonucci, R. R. J., & Miller, J. S. 1985, *ApJ*, 297, 621
- Baba, H., Yasuda, N., Ichikawa, S.-I. et al. 2002, in *ASP Conf. Ser.* 281: ADASS XI, ed. Bohlender, D.A., Durand, D. & Handley, T.H., 298
- Bakos, J., & Trujillo, I. 2012, arXiv:1204.3082
- Baldwin, J. A., Phillips, M. M., & Terlevich, R. 1981, *PASP*, 93, 5
- Barnes, J. E., & Hernquist, L. 1992, *Nature*, 360, 715
- Bertin, E., & Arnouts, S. 1996, *A&AS*, 117, 393
- Binney, J., & Tremine, S. 1987, *Galactic Dynamics* (Princeton University Press), chap. 7
- Blanton, M. R., & Roweis, S. 2007, *AJ*, 133, 734
- Bosch, J., Armstrong, R., Bickerton, S., et al. 2017, *PASJ*, in press (arXiv:1705.06766)
- Cecil, G., Dopita, M. A., Groves, B., Wilson, A. S., Ferruit, P., Pecontal, E., & Binette, L. 2002, *ApJ*, 568, 627
- Coleman, G. D., Wu, C.-C., & Weedman, D. W. 1980, *ApJS*, 43, 393
- Chambers, K. C., Magnier, E. A., Metcalfe, N., et al. 2016, arXiv:1612.05560
- Chonis, T. S., Martínez-Delgado, D., Gabany, R. J., et al. 2011, *AJ*, 142, 166
- de Vaucouleurs, G., et al. 1991, *Third Reference Catalog of Bright Galaxies (RC3)*
- Dickel, J. R., & Rood, H. J. 1978, *ApJ*, 223, 391
- Duc, P.-A., Paudel, S., McDermid, R. M., et al. 2014, *MNRAS*, 440, 1458
- Duc, P.-A., Cuillandre, J.-C., Karabal, E., et al. 2015, *MNRAS*, 446, 120
- Fukugita, M., Shimasaku, K., & Ichikawa, T. 1995, *PASP*, 107, 945
- Fukugita, M., Nakamura, O., Okamura, S., et al. 2007, *AJ*, 134, 579
- Furuya, R. S., & Taniguchi, Y. 2016, *PASJ*, 68, 103
- Gavazzi, G., Donati, A., Cucciati, O., et al. 2005, *A&A*, 430, 411
- Graham, A. W., & Guzmán, R. 2003, *AJ*, 125, 2936
- Graham, A. W., & Driver, S. P. 2005, *PASA*, 22, 118
- García-Burillo, S., Combes, F., Usero, A., et al. 2014, *A&A*, 567, A125
- García-Lorenzo, B., Mediavilla, E., Arribas, S., & del Burgo, C. 1997, *ApJ*, 483, L99
- Gallimore, J. F., Baum, S. A., O’Dea, C. P., Brinks, E., & Pedlar, A. 1996, *ApJ*, 462, 740
- Gallimore, J. F., Henkel, C., Baum, S. A., et al. 2001, *ApJ*, 556, 694
- Gallimore, J. F., Baum, S. A., & O’Dea, C. P. 2004, *ApJ*, 613, 794
- Goto, T. 2005, *MNRAS*, 357, 937
- Greenhill, L. J., Gwinn, C. R., Antonucci, R., & Barvainis, R. 1996, *ApJL*, 472, L21
- Häussler, B., McIntosh, D. H., Barden, M., et al. 2007, *ApJS*, 172, 615
- Holwerda, B. W., Muñoz-Mateos, J.-C., Comerón, S., et al. 2014, *ApJ*, 781, 12
- Hopkins, P. F., Hernquist, L. C., Cox, T. J., & Keres, D. 2008, *ApJS*, 175, 356
- Huchra, J. P., & Geller, M. J. 1982, *ApJ*, 252, 437
- Ji, I., Peirani, S., & Yi, S. K. 2014, *A&A*, 566, A97
- Kazantzidis, S., Bullock, J. S., Zentner, A. R., Kravtsov, A. V., & Moustakas, L. A. 2008, *ApJ*, 688, 254-276
- Kauffmann, G., Heckman, T. M., Tremonti, C., et al. 2003, *MNRAS*, 346, 1055
- Khan, F. M., Preto, M., Berczik, P., et al. 2012, *ApJ*, 749, 147
- Kewley, L. J., Dopita, M. A., Sutherland, R. S., Heisler, C. A., Trevena, J. 2001, *ApJ*, 556, 121
- Koda, J., Yagi, M., Yamanoi, H., & Komiyama, Y. 2015, *ApJL*, 807, L2
- Komiyama, Y., Sekiguchi, M., Kashikawa, N., et al. 2002, *ApJS*, 138, 265
- Kormendy, J., & Ho, L. C. 2013, *ARA&A*, 51, 511
- Lang, D., Hogg, D. W., Mierle, K., Blanton, M., Roweis, S. 2010, *AJ*, 139, 1782
- Malkan, M. A., Gorjian, V., & Tam, R. 1998, *ApJS*, 117, 25
- Lodato, G., & Bertin, G. 2003, *A&A*, 398, 517
- Martínez-Delgado, D., Peñarrubia, J., Gabany, R. J., et al. 2008, *ApJ*, 689, 184
- Martínez-Delgado, D., Gabany, R. J., Crawford, K., et al. 2010, *AJ*, 140, 962
- Martínez-Delgado, D., Romanowsky, A. J., Gabany, R. J., et al. 2012, *ApJL*, 748, L24
- Martínez-Delgado, D., D’Onghia, E., Chonis, T. S., et al. 2015, *AJ*, 150, 116
- Merritt, A., van Dokkum, P., Danieli, S., et al. 2016, *ApJ*, 833, 168
- Miller, B., Gallo, E., Henny, E., et al. 2015, *ApJ*, 799, id.98
- Miskolczi, A., Bomans, D. J., & Dettmar, R.-J. 2011, *A&A*, 536, A66
- Miyazaki, S., Komiyama, Y., Sekiguchi, M., et al. 2002, *PASJ*, 54, 833
- Miyazaki, S., Komiyama, Y., Nakaya, H., et al. 2012, *Proc. SPIE*, 8446, 84460Z
- Miyoshi, M., Moran, J., Herrnstein, J., Greenhill, L., Nakai, N., Diamond, P., & Inoue, M. 1995, *Nature*, 373, 127
- Mobasher, B., Bridges, T. J., Carter, D., et al. 2001, *ApJS*, 137, 279
- Murayama, T., & Taniguchi, Y. 1997, *PASJ*, 49, L13
- Newberg, H. J., Yanny, B., Rockosi, C., et al. 2002, *ApJ*, 569, 245
- Peng, C. Y., Ho, L. C., Impey, C. D., & Rix, H.-W. 2002, *AJ*, 124, 266
- Peng, C. Y., Ho, L. C., Impey, C. D., & Rix, H.-W. 2010, *AJ*, 139, 2097
- Purcell, C. W., Bullock, J. S., Tollerud, E. J., Rocha, M., & Chakrabarti, S. 2011, *Nature*, 477, 301
- Robert, M. S., & Heynes, M. P. 1994, *ARA&A*, 32, 115
- Sánchez-Portal, M., Díaz, Á. I., Terlevich, R., et al. 2000, *MNRAS*, 312, 2
- Sanders, D. B., Soifer, B. T., Elias, J. H., et al. 1988, *ApJ*, 325, 74

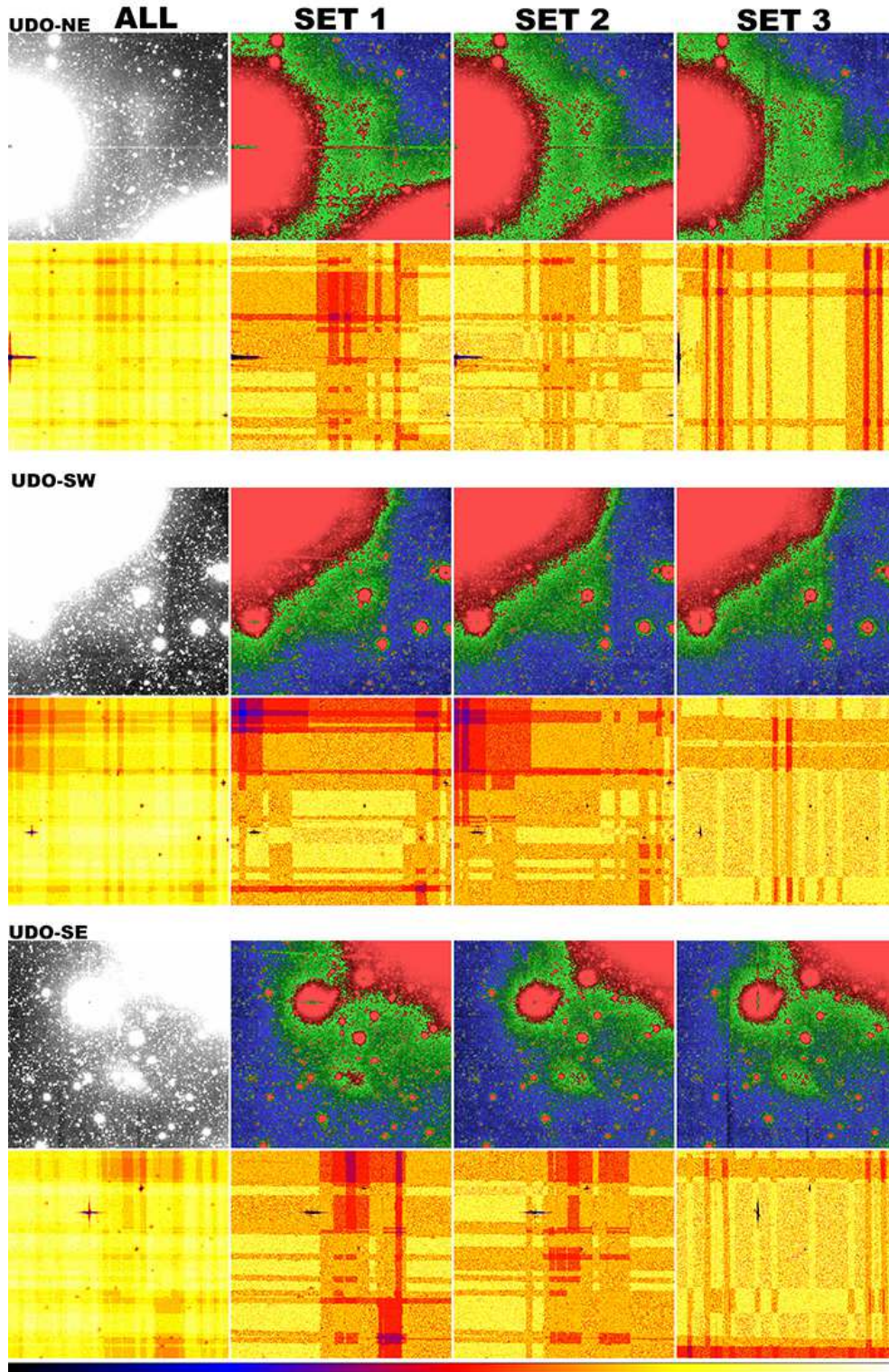


Fig. 8. Comparison of the UDO shape among the subsamples. Each set of 8 tiled images at the top, middle, and bottom shows the result for UDO-SE, UDO-NE, and UDO-SW, respectively. In each grouped images, the top left image (monochrome) shows the image with all the 33 frames combined. The next three images are the result for the subsets, each of which is the average of the 11 frames. At the bottom of each panel, we show the exposure map for each combined subset, with the scale bar at the bottom of the figure (left= 0%, right= 100% of the total exposures for each subset).

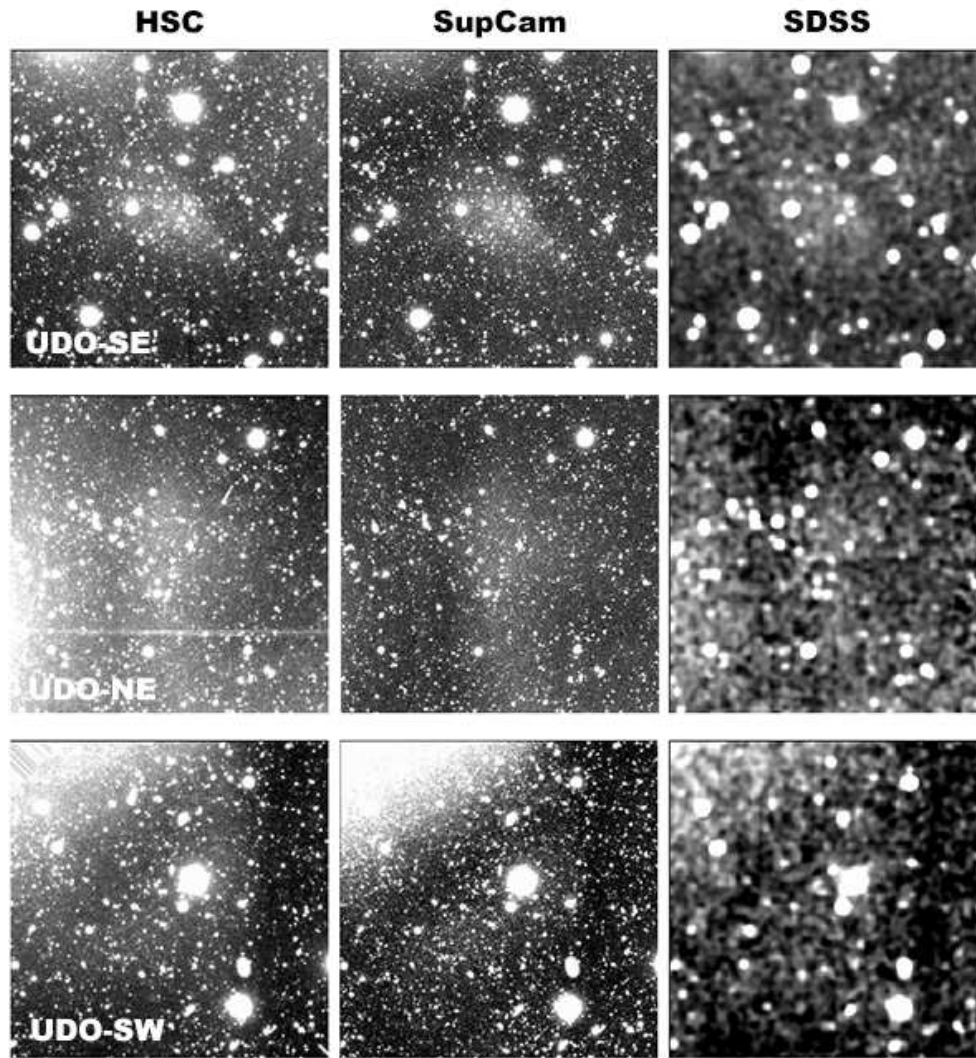


Fig. 9. Comparison of the appearance of the UDOs on the images taken by the HSC (left), the Suprime-Cam (middle), and the SDSS DR12 (right: here we use the r -band data). Note that the SDSS images are after applying the smoothing (3×3 pixels block average + the Gaussian smoothing with $\sigma = 2$ pixels) to show the faintest features. Also note that the SDSS data are largely affected by the poor sky subtraction, and thus any morphological information from the data may not be reliable. However, we can barely see a hint of these UDOs in the images.

Schawinski, K., Dowlin, N., Thomas, D., Urry, C. M., & Edmondson, E. 2010, *ApJL*, 714, L108
 Sérsic, J. L. 1968, *Atlas de galaxias australes*, Cordoba, Argentina: Observatorio Astronomico
 Seyfert, C. K. 1943, *ApJ*, 97, 28
 Schmitt, H. R., & Kinney, A. L. 1996, *ApJ*, 463, 498
 Smirnova, A. A., Moiseev, A. V., & Afanasiev, V. L. 2010, *MNRAS*, 408, 400
 Storchi-Bergamnn, T., et al. 2012, *ApJ*, 755, 87
 Swaters, R. A., Sancisi, R., van Albada, T. S., & van der Hulst, J. M. 2011, *ApJ*, 729, 118
 Taniguchi, Y. 1997, *ApJ*, 487, L17
 Taniguchi, Y. 1999, *ApJ*, 524, 65
 Taniguchi, Y. 2013, *Galaxy Mergers in an Evolving Universe*, ed. Sun, W-H; Xu, C. K.; Scoville, N. Z.; & Sanders, D. B. (San Francisco: ASP), 477, 265

Taniguchi, Y., & Murayama, T. 1998, *ApJL*, 501, L25
 Taniguchi, Y., & Shioya, Y. 1998, *ApJ*, 501, L167
 Taniguchi, Y., & Wada, K. 1996, *ApJ*, 469, 581
 Telesco, C. M., et al. 1984, *ApJ*, 282, 427
 Urry, C. M., & Padovani, P. 1995, *PASP*, 107, 803
 van Dokkum, P. G., Abraham, R., Merritt, A., et al. 2015, *ApJL*, 798, L45
 van Dokkum, P. G., Romanowsky, A. J., Abraham, R., et al. 2015, *ApJL*, 804, L26
 van Dokkum, P. G., Abraham, R., Brodie, J., et al. 2016, *ApJL*, 828, L6
 Willett, K. W., Lintott, C. J., Bamford, S. P., et al. 2013, *MNRAS*, 435, 2835
 Yagi, M., Suzuki, N., Yamanoi, H. et al. 2013, *PASJ*, 65, 22
 Yagi, M., Koda, J., Komiyama, Y. & Yamanoi, H. 2016, *ApJS*, 225, 11
 Yagi, M., Yoshida, M., Komiyama, H. et al. 2017, *ApJ*, 839, 65
 Yoshida, M., Yagi, M., Ohyama, Y., et al. 2016, *ApJ*, 820, 48